Crossover from Single-Step Tunneling to Multistep Hopping for Molecular Triplet Energy Transfer

Josh Vura-Weis, *et al.*

Science **328**, 1547 (2010);
DOI: 10.1126/science.1189354

polarizability. By symmetry, this modulation should arise if the driving electromagnetic wave contains an electric-field component along the Ti-O bond. Consequently, it is only observed with a p-polarized probe beam. For the s-polarized case, the SHG response arises mainly from the PbSe quantum dots, and the coherent phonon mode at 70 cm^{-1} dominates.

We take the coherent surface phonon attributed to TiO_2 as further evidence for hot-electron transfer. Such vibrations can be excited when electric fields near the surface are activated by optical pulses shorter than the vibrational period (*33*). Electron transfer across the PbSe-TiO_2 interface within the 50-fs width of the excitation pulse establishes an interfacial electric field faster than the characteristic response time of the surface atoms. These atoms subsequently find themselves in a vibrationally excited state of the new electric-field–induced minimum energy surface configuration. Time-domain fitting of an appropriate model function to the data in Fig. 4A (see fig. S11) reveals that the initial phase of this vibration is a cosine, consistent with a displacive excitation mechanism (see SOM text 3). The phase coherence of these collective motions is then lost over time because of elastic and inelastic scattering with bulk phonons.

These results indicate that hot-electron transfer from semiconductor nanocrystals to a technologically relevant electron acceptor is possible. This effect is expected to be of general relevance to other semiconductor nanocrystals and electron and hole conductors, provided the hot electrons and holes possess sufficiently long lifetimes and the interfaces are properly controlled to enable ultrafast charge transfer. Moreover, if hot-electron (hole) transfer can be controlled to occur in very narrow energy windows to also minimize loss in the electron (hole) conductor, the highly efficient hot-carrier solar cell may be realized.

References and Notes

1. W. Shockley, H. J. Queisser, *J. Appl. Phys.* **32**, 510 (1961).
2. R. T. Ross, A. J. Nozik, *J. Appl. Phys.* **53**, 3813 (1982).
3. A. P. Alivisatos, *Science* **271**, 933 (1996).
4. A. J. Nozik, *Annu. Rev. Phys. Chem.* **52**, 193 (2001).
5. K. Mukai, M. Sugawara, in *Self-Assembled InGaAs/GaAs Quantum Dots* (Academic Press, San Diego, CA, 1999), vol. 60, pp. 209–239.
6. A. Pandey, P. Guyot-Sionnest, *Science* **322**, 929 (2008).
7. A. Pandey, P. Guyot-Sionnest, *J. Phys. Chem. Lett.* **1**, 45 (2010).
8. A. J. Nozik, *Physica E* **14**, 115 (2002).
9. N. A. Anderson, T. Q. Lian, *Annu. Rev. Phys. Chem.* **56**, 491 (2005).
10. J. L. Blackburn *et al.*, *J. Phys. Chem. B* **109**, 2625 (2005).
11. I. Robel, V. Subramanian, M. Kuno, P. V. Kamat, *J. Am. Chem. Soc.* **128**, 2385 (2006).
12. B. R. Hyun *et al.*, *ACS Nano* **2**, 2206 (2008).
13. S. Y. Jin, T. Q. Lian, *Nano Lett.* **9**, 2448 (2009).
14. Y. R. Shen, *Nature* **337**, 519 (1989).
15. M. Omote *et al.*, *J. Phys. Cond. Mat.* **17**, S175 (2005).
16. E. A. McArthur, K. B. Eisenthal, *J. Am. Chem. Soc.* **128**, 1068 (2006).
17. D. V. Talapin, C. B. Murray, *Science* **310**, 86 (2005).
18. F. W. Wise, *Acc. Chem. Res.* **33**, 773 (2000).
19. See supporting material on *Science* Online.
20. D. Yu, C. J. Wang, P. Guyot-Sionnest, *Science* **300**, 1277 (2003).
21. J. M. Luther *et al.*, *ACS Nano* **2**, 271 (2008).
22. K. J. Williams *et al.*, *ACS Nano* **3**, 1532 (2009).
23. T. F. Heinz, in *Nonlinear Surface Electromagnetic Phenomena*, H. Ponrath, G. Stegeman, Eds. (Elsevier, Amsterdam, 1991), pp. 353–416.
24. R. M. Corn, D. A. Higgins, *Chem. Rev.* **94**, 107 (1994).
25. O. A. Aktsipetrov *et al.*, *Phys. Rev. B* **60**, 8924 (1999).
26. A. Nahata, T. F. Heinz, *Opt. Lett.* **23**, 67 (1998).
27. J. C. Johnson *et al.*, *Nano Lett.* **4**, 197 (2004).
28. R. D. Schaller *et al.*, *Phys. Rev. Lett.* **95**, 196401 (2005).
29. E. Hendry, F. Wang, J. Shan, T. F. Heinz, M. Bonn, *Phys. Rev. B* **69**, 081101 (2004).
30. O. V. Prezhdo, W. R. Duncan, V. V. Prezhdo, *Prog. Surf. Sci.* **84**, 30 (2009).
31. R. N. Hall, J. H. Racette, *J. Appl. Phys.* **32**, 2078 (1961).
32. R. Lindsay *et al.*, *Phys. Rev. Lett.* **94**, 246102 (2005).
33. Y. M. Chang, L. Xu, H. W. K. Tom, *Phys. Rev. Lett.* **78**, 4649 (1997).

34. We thank K. S. Leschkies, A. Wolcott, C. Nelson, and G. Haugstad for assistance with PbSe nanocrystal synthesis and atomic force microscopy imaging. This work was supported by the U.S. Department of Energy (DE-FG02-07ER46468). Partial support from the NSF Nanoscale Interdisciplinary Research Team (NIRT) program (CBET-0506672) and the Materials Research Science and Engineering Center (MRSEC) programs (DMR-0819885) in the form of student assistantships to B.A.T. and W.A.T. are acknowledged. W.A.T. received support from a University of Minnesota Doctoral Dissertation Fellowship.

Supporting Online Material

www.sciencemag.org/cgi/content/full/328/5985/1543/DC1
Materials and Methods
SOM Text
Figs. S1 to S11
Table S1
References

3 December 2009; accepted 4 May 2010
10.1126/science.1185509

Crossover from Single-Step Tunneling to Multistep Hopping for Molecular Triplet Energy Transfer

Josh Vura-Weis,[1] Sameh H. Abdelwahed,[2] Ruchi Shukla,[2] Rajendra Rathore,[2]* Mark A. Ratner,[1]* Michael R. Wasielewski[1]*

Triplet energy transfer (TT), a key process in molecular and organic electronics, generally occurs by either strongly distance-dependent single-step tunneling or weakly distance-dependent multistep hopping. We have synthesized a series of π-stacked molecules consisting of a benzophenone donor, one to three fluorene bridges, and a naphthalene acceptor, and studied the rate of TT from benzophenone to naphthalene across the fluorene bridge using femtosecond transient absorption spectroscopy. We show that the dominant TT mechanism switches from tunneling to wire-like hopping between bridge lengths 1 and 2. The crossover observed for TT can be determined by direct observation of the bridge-occupied state.

The rapid and efficient transport of energy and charge over tens to hundreds of nanometers in molecules underlies the performance of devices such as organic photovoltaics, thin-film transistors, and light-emitting diodes. Charge and energy transport is also crucial to many biological processes, such as long-distance electron transfer in proteins (*1*) and the quenching of triplets in the bacterial photosynthetic reaction center by energy transfer cascades. (*2*) The study of charge transfer (CT) and triplet energy transfer (TT) in donor-bridge-acceptor (D-B-A) systems has demonstrated two general transport mechanisms—strongly distance-dependent single-step tunneling and weakly distance-dependent multistep hopping, which is also known as wire-like transport (*3*). Optimizing TT efficiency is particularly important for improving organic and polymer light-emitting diode (OLED/PLED) performance, because injection of charge into the active layer of these devices generally leads to a 3:1 ratio of triplet to singlet excitons through spin statistics (*4*, *5*), although the singlet exciton population may be higher in π-conjugated polymers (*6*). TT in PLEDs occurs both within and between chains (*7*), so that transport through noncovalent π-stacked molecules is important.

A major goal is to design molecules that exhibit multistep hopping in which charge or energy moves from a donor to the bridge and then later to the acceptor. Several CT studies have shown a crossover from tunneling to hopping as the bridge length increased, which

[1]Department of Chemistry and Argonne-Northwestern Solar Energy Research (ANSER) Center, Northwestern University, Evanston, IL 60208, USA. [2]Department of Chemistry, Marquette University, Post Office Box 1881, Milwaukee, WI 53201, USA.

*To whom correspondence should be addressed: rajendra.rathore@marquette.edu (R.R.); ratner@chem.northwestern.edu (M.A.R.); m-wasielewski@northwestern.edu (M.R.W.)

has shed light on the interplay between electronic coupling and D-B and B-A energy matching necessary for rapid charge transfer (*8*–*11*). Because the oxidized/reduced bridge molecules are generally poor chromophores (*12*), the crossover in mechanism has been deduced from a "kink" in plots of the transfer rate versus D-A distance or from a delay between the appearance of D^+ and the appearance of A^-, as opposed to direct spectroscopic measurements of the bridge-occupied state. Although synthetic analogs of the triplet energy cascades found in nature have been prepared (*13*, *14*), a switch in TT mechanism as a function of bridge length has not yet been demonstrated.

We present direct evidence for a change in mechanism from single-step tunneling to multistep hopping for TT determined by spectroscopic detection of the bridge-occupied state. As our D-B-A system, we have synthesized molecules with a benzophenone triplet energy donor (Bp), polyfluorene bridges (F_n, where n = 1 to 3), and a naphthalene acceptor (Nap) (Fig. 1A). These are constrained to a π-stacked geometry through methylene linkers. The cofacially arrayed polyfluorene bridges have been shown by ^{1}H NMR (nuclear magnetic resonance) spectroscopy to remain π-stacked in solution, and single-crystal x-ray crystallography has shown that the fluorenes are separated by ~3.0 Å at their closest contact (*15*). All of the molecules we report have been fully characterized by NMR and high-resolution mass spectrometry, and the structure of a representative triad was also confirmed by x-ray crystallography (Fig. 1B). Synthetic details are given in the supporting online material (*16*).

The triplet energy levels of Bp, F_n, and Nap (Fig. 1C) were determined from phosphorescence spectroscopy and Configuration Interaction Singles (CIS) calculations (*16*). The ^3F_n energy of 2.8 eV was always between that of ^{3}Bp (3.0 eV) and ^{3}Nap (2.6 eV). The ^3F_n energy was independent of the number of fluorenes, indicating weak coupling between the fluorene monomers and a lack of triplet delocalization. In contrast, the triplet energy level of linearly conjugated oligofluorene decreases from 2.86 to 2.25 eV as the length increases from one to three monomers because of increased delocalization of the wave function (*17*).

We monitored TT using femtosecond transient absorption spectroscopy. A 150-fs, 350-nm laser pulse selectively excited Bp, and transient spectra were measured with a white-light continuum probe pulse. The total instrument response function was 180 fs. The three-dimensional (3D) transient absorption spectra for each molecule are shown in Fig. 2. The initially created ^{1*}Bp state absorbed at 580 nm (*18*) and was converted by intersystem crossing to ^{3}Bp, which absorbed at 535 nm. In the Bp-F_n model compounds, the triplet energy then transferred from ^{3}Bp to the F_n bridge, as revealed by the absorptive feature at ~400 nm for all molecules and an additional peak at ~585 nm for F_2 and F_3. The lack of 585-nm absorption in $^3F_1$ is consistent with the $T_1 \rightarrow T_n$ spectra of linearly conjugated fluorenes, which show only a 385-nm peak for one fluorene but an additional 690-nm peak for longer oligomers (*17*).

Because overlapping spectral features are present, we determined the intersystem crossing time constant τ_{isc} (^{1*}Bp→^{3}Bp) and bridge injection times τ_{inj} (^{3}Bp→^3F_n) using a global fitting routine that incorporates a sequential kinetic model. The global fits of the Bp-F_n transient spectra (Fig. 2, A to C) gave τ_{isc} = 6 ps and τ_{inj} = 156, 119, and 104 ps for Bp-F_1, Bp-F_2, and Bp-F_3, respectively (*19*). The value of τ_{isc} is constant for all molecules studied and will be ignored for the remainder of the discussion, as it is much faster than all other processes studied. Also we report time constants instead of rate constants ($\tau = 1/k$) except in rate equations. In each of these fits, spectral and kinetic slices of the reconstructed data are nearly superimposable with the corresponding slices of the experimental data.

The rate of TT may be roughly described in the nonadiabatic, high-temperature Marcus formalism (*20*–*24*)

$$k = \frac{2\pi}{\hbar} V^2 \sqrt{\frac{1}{4\pi\chi k_B T}} e^{\frac{-(\Delta G^\circ + \chi)^2}{4\chi k_B T}} \quad (1)$$

where ΔG° is the free energy change, χ is the reorganization energy arising from Huang-Rhys factors associated with excitation transfer (*22*), and V is the electronic coupling between D and A, which depends on orbital overlap and therefore scales exponentially with distance. This scaling is influenced by the intervening medium and is characterized by a factor β such that $k \propto \exp(-\beta * R_{DA})$, where R_{DA} is the donor-acceptor distance. The

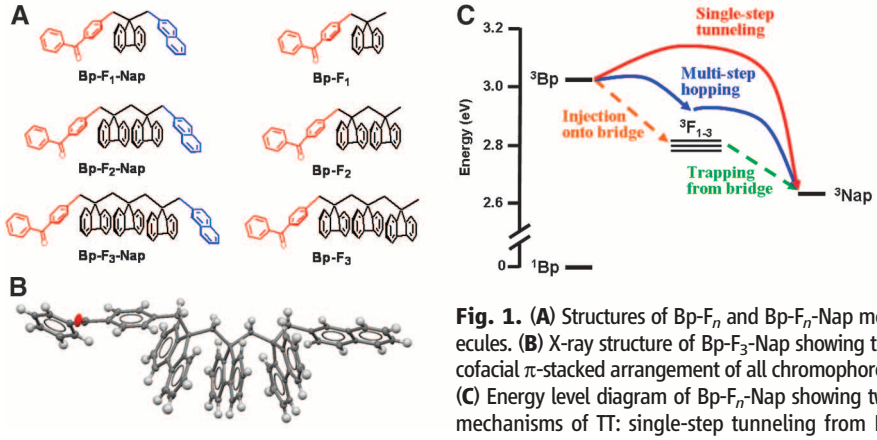

Fig. 1. (**A**) Structures of Bp-F_n and Bp-F_n-Nap molecules. (**B**) X-ray structure of Bp-F_3-Nap showing the cofacial π-stacked arrangement of all chromophores. (**C**) Energy level diagram of Bp-F_n-Nap showing two mechanisms of TT: single-step tunneling from Bp to Nap, or multistep hopping consisting of injection onto the F_n bridge followed by trapping by Nap. The triplet energy of the F_n bridges is independent of n to within 0.02 eV.

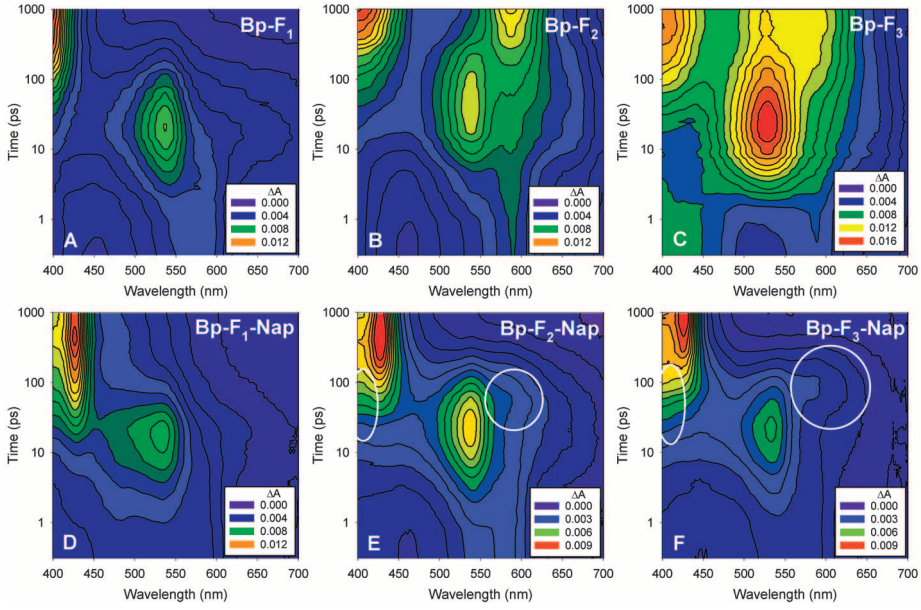

Fig. 2. Transient absorption spectra of Bp-F_n (**A** to **C**) and Bp-F_n-Nap (**D** to **F**). White ovals identify absorption due to the ^3F_n bridge-occupied state.

length dependence of τ_{inj} cannot be explained by differences in $\Delta G°$ or χ, because the bridge energies are nearly degenerate. Instead, we postulate that the Bp triplet can tunnel to any of the n bridge sites (i.e., to site 1 or 2 for Bp-F_2), with the observed rate for Bp-F_2 and Bp-F_3 being the sum of the two or three individual rates. As discussed in the supporting online text (*16*), such a model leads to a β value of 0.36 $Å^{-1}$. This is smaller than might be expected for a π-stacked system, although it is within the range observed for TT across conjugated bridges (*25*–*28*). We suspect that this low β value is due to the compressed π stack that leads to strong electronic coupling between the different sites; a similar effect has been seen for charge transfer through a benzene stack (*29*).

The transient spectrum of the Bp-F_1-Nap donor-bridge-acceptor molecule (Fig. 2D) showed the same $^{1*}Bp \rightarrow {}^3Bp$ progression from 585 to 535 nm as Bp-F_n, followed by loss of the ^3Bp peak and growth of absorption at 425 nm that is characteristic of ^3Nap. We fitted the $^{1*}Bp \rightarrow {}^3Bp \rightarrow {}^3Nap$ process using the two-step model described above and obtained a total TT time τ_{tot} ($^3Bp \rightarrow {}^3Nap$) of 62 ps, again with excellent agreement between the experimental and reconstructed data. This time is surprising, because it is much faster than the 156 ps triplet injection time for Bp-F_1. Full TT must occur at least partially through a single-step tunneling mechanism, and the observed rate k_{tot} will be the sum of the rates of hopping and tunneling processes ($k_{tot} = k_{tun} + k_{hop}$). Because there was no evidence for buildup of triplet on the F_1 bridge, we can assume that in Bp-F_1-Nap, the trapping rate k_{trap} was much faster than k_{inj}, and thus $k_{hop} \approx k_{inj}$. Using $\tau_{hop} = 156$ ps and $\tau_{tot} = 62$ ps, we calculated a tunneling time τ_{tun} of 104 ps, which results in quantum yields of 60% for single-step tunneling and 40% for hopping. The relative free energy changes of the two processes causes direct tunneling from Bp to Nap to be faster than triplet injection onto F_1. A straightforward application of Marcus theory can be used to explain this result (*16*).

Unlike the transient spectra of Bp-F_1-Nap, those of Bp-F_2-Nap and Bp-F_3-Nap could not be fit well using a two-step $^{1*}Bp \rightarrow {}^3Bp \rightarrow {}^3Nap$ model. The reconstructed spectra underestimate a 585-nm shoulder at intermediate times, as shown in Fig. 3A for Bp-F_2-Nap. Absorption from 400 to 420 nm is also underrepresented in the fit. Inspection of the average residual (data minus fit) from 50 to 200 ps shows a strong resemblance to the $^3F_2$ spectrum seen at long times in the transient absorption of Bp-F_2, with peaks at 585 and ~400 nm (Fig. 3B). This shows that the $^3F_2$ bridge state is occupied at intermediate times. The dips in the residual at 430 and 530 nm correspond to ^3Nap and ^3Bp absorption that is overrepresented in the fit.

We therefore extended the global fit to use a three-step $^{1*}Bp \rightarrow {}^3Bp \rightarrow {}^3F_n \rightarrow {}^3Nap$ kinetic model, where the ^3F_n state represents the triplet localized on any of the spectroscopically indistinguishable bridge sites. Because of the large number of fitting parameters, the $^3Bp \rightarrow {}^3F_n$ time constants were fixed at the values obtained from the Bp-F_n model complexes. The 400-nm and 585-nm absorption at intermediate times is now well represented in the fit (Fig. 3C). Trapping times τ_{trap} for the $^3F_n \rightarrow {}^3Nap$ process were fit as 74 ps and 179 ps for Bp-F_2-Nap and Bp-F_3-Nap, respectively. The slower trapping time for Bp-F_3-Nap is consistent with the qualitative observation that the ^3F_n features at 400 and 585 nm are more prominent in its transient spectra because of a higher population of the bridge-occupied state. Because triplet injection preferentially populates the bridge sites closest to Bp, adding more sites necessarily slows τ_{trap}, either because the triplet takes time to migrate along the bridge or because direct trapping from the distant bridge site is slow. Although we have modeled the $^3F_n \rightarrow {}^3Nap$ step as a simple rate process that depends on a single rate constant and the total population of all bridge sites, in reality this step is certainly more complex. Given the lack of information on the exact location of the triplet within the F_n bridge, we feel this is a reasonable approximation.

Finally, we constructed a plot showing the evolution of the total, hopping, and tunneling rates as a function of bridge length to illustrate the crossover between tunneling-dominated behavior and hopping-dominated behavior. Given the rates measured above, along with the calculated β value of 0.36$Å^{-1}$, we estimate tunneling times τ_{tun} for Bp-F_2-Nap and Bp-F_3-Nap as 310 and 900 ps, respectively. We calculate phenomenological hopping and total rates k_{hop} and k_{tot} by simulating the ^3Nap population as a function of time and fitting it to a single-exponential rise. For k_{hop} we omit the direct $^3Bp \rightarrow {}^3Nap$ pathway, whereas for k_{tot} all pathways are included. Figure 4 shows the microscopic k_{tun}, k_{inj}, and k_{trap} and phenomenological k_{hop} and k_{tot} rates as a function of Bp-Nap distance and number of fluorenes n.

The crossover between tunneling and hopping as the dominant mechanism occurs between n = 1 and 2, where the percentage of population transferred by single-step tunneling drops from 60% to 28%. Two factors influence this crossover. The primary cause is the steep drop in k_{tun} that results from the exponential distance dependence of orbital overlap. In addition, k_{inj} rises because of the addition of a second bridge site to which the energy can transfer. Because k_{trap} falls more sharply than k_{inj} rises, the net hopping rate k_{hop} decreases slightly. At n = 3, the trapping rate becomes rate-limiting for k_{hop}. At this distance k_{tot} is further dominated by k_{hop}, with 90% of the TT going through the hopping pathway.

Our direct study of the crossover between single-step tunneling and multistep hopping as the bridge length increases shows that while the bridge is energetically accessible in all cases,

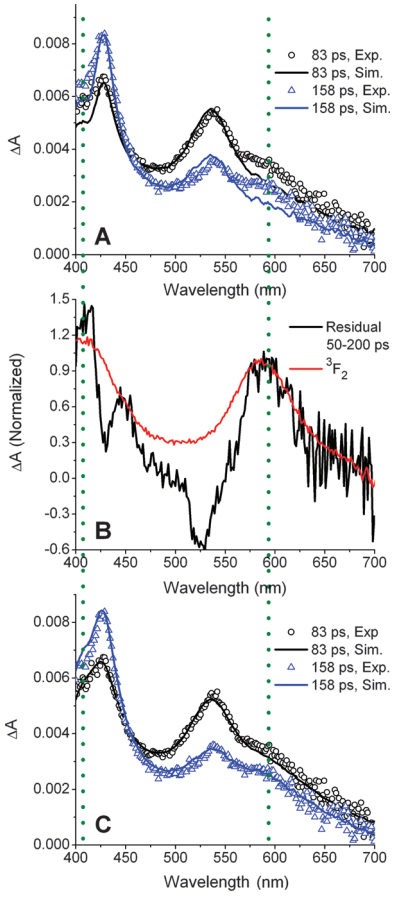

Fig. 3. (**A**) Experimental and reconstructed transient spectra of Bp-F_2-Nap at 83 and 158 ps using a two-step $^{1*}Bp \rightarrow {}^3Bp \rightarrow {}^3Nap$ model. The fit is poor at 400 and 585 nm, as highlighted by the dotted green line. (**B**) Average residual (data-fit) from 50 to 200 ps versus $^3F_2$ spectrum, both of which peak at 400 and 585 nm. (**C**) Experimental and reconstructed transient spectra of Bp-F_2-Nap at 83 and 158 ps using a three-step $^{1*}Bp \rightarrow {}^3Bp \rightarrow {}^3F_2 \rightarrow {}^3Nap$ model. Addition of the $^3F_2$ intermediate leads to excellent fits at those wavelengths.

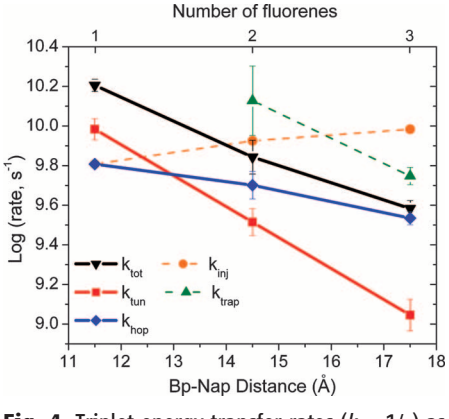

Fig. 4. Triplet energy transfer rates ($k = 1/\tau$) as a function of Bp-Nap distance. Single-step tunneling dominates for n = 1, whereas multistep hopping dominates for n = 2 or 3. Error bars are the standard deviation of three measurements (*16*).

tunneling is preferred for the shortest bridge length because of the large free-energy change between D and A. At longer distances, the poor scaling of direct tunneling favors a stepwise mechanism. Triplet energy transfer through π-stacked molecules is common in organic light-emitting diodes, and this intermediate regime between the strong distance dependence of tunneling and weak distance dependence of hopping may prove useful in understanding and designing energy transfer pathways in such devices.

References and Notes

1. H. B. Gray, J. R. Winkler, *Annu. Rev. Biochem.* **65**, 537 (1996).
2. L. Takiff, S. G. Boxer, *J. Am. Chem. Soc.* **110**, 4425 (1988).
3. P. F. Barbara, T. J. Meyer, M. A. Ratner, *J. Phys. Chem.* **100**, 13148 (1996).
4. M. A. Baldo, D. F. O'Brien, M. E. Thompson, S. R. Forrest, *Phys. Rev. B* **60**, 14422 (1999).
5. V. Cleave, G. Yahioglu, P. L. Barny, R. H. Friend, N. Tessler, *Adv. Mater.* **11**, 285 (1999).
6. M. Wohlgenannt, Z. V. Vardeny, *J. Phys. Condens. Matter* **15**, R83 (2003).
7. H. H. Liao *et al.*, *Phys. Rev. B* **74**, 245211 (2006).
8. W. B. Davis, W. A. Svec, M. A. Ratner, M. R. Wasielewski, *Nature* **396**, 60 (1998).
9. R. H. Goldsmith *et al.*, *Proc. Natl. Acad. Sci. U.S.A.* **102**, 3540 (2005).
10. E. A. Weiss *et al.*, *J. Am. Chem. Soc.* **126**, 5577 (2004).
11. F. D. Lewis *et al.*, *J. Am. Chem. Soc.* **128**, 791 (2006).
12. M. U. Winters, K. Pettersson, J. Mårtensson, B. Albinsson, *Chemistry - A European Journal* **11**, 562 (2005).
13. D. Gust *et al.*, *J. Photochem. Photobiol. B* **43**, 209 (1998).
14. R. E. Palacios *et al.*, *Chem. Phys. Chem.* **6**, 2359 (2005).
15. R. Rathore, S. H. Abdelwahed, I. A. Guzei, *J. Am. Chem. Soc.* **125**, 8712 (2003).
16. Materials and methods are available as supporting material on *Science* Online.
17. D. Wasserberg, S. P. Dudek, S. C. J. Meskers, R. A. J. Janssen, *Chem. Phys. Lett.* **411**, 273 (2005).
18. M. Montalti, A. Credi, L. Prodi, M. T. Gandolfi, *Handbook of Photochemistry, Third Edition* (Taylor & Francis, Boca Raton, FL, 2006).
19. Errors are shown in Fig. 4 and are about <5% for injection times and 10 to 30% for all other times. See table S1 for all times and errors.
20. R. A. Marcus, *Annu. Rev. Phys. Chem.* **15**, 155 (1964).
21. M. E. Sigman, G. L. Closs, *J. Phys. Chem.* **95**, 5012 (1991).
22. The Marcus treatment was developed to describe electron transfer but is also valid for TT, which is often described as a "double exchange" or "Dexter exchange" (*23*) process. Energy transfer arises from electron tunneling among sites due to two-electron exchange integrals, accompanied by reorganizational energy in the nuclear motion (Huang-Rhys factors). Note that we have used the variable χ for the reorganization term to distinguish this process from charge transfer, where λ is used. Other parallels between energy and electron transfer have been shown (*24*).
23. D. L. Dexter, *J. Chem. Phys.* **21**, 836 (1953).
24. J. J. Hopfield, *Proc. Natl. Acad. Sci. U.S.A.* **71**, 3640 (1974).
25. J. Andreasson, J. Kajanus, J. Mårtensson, B. Albinsson, *J. Am. Chem. Soc.* **122**, 9844 (2000).
26. A. C. Benniston, V. Grosshenny, A. Harriman, R. Ziessel, *Angew. Chem. Int. Ed. Engl.* **33**, 1884 (1994).
27. A. Harriman, A. Khatyr, R. Ziessel, A. C. Benniston, *Angew. Chem. Int. Ed.* **39**, 4287 (2000).
28. B. Albinsson, J. Mårtensson, *J. Photochem. Photobiol. Photochem. Rev.* **9**, 138 (2008).
29. Y. K. Kang, I. V. Rubtsov, P. M. Iovine, J. X. Chen, M. J. Therien, *J. Am. Chem. Soc.* **124**, 8275 (2002).

30. J.V.W. thanks R. H. Goldsmith for assistance with Matlab and helpful discussions. This work was supported by the Chemical Sciences, Geosciences, and Biosciences Division, Office of Basic Energy Sciences, Department of Energy, under grant DE-FG02-99ER14999 (M.R.W.), NSF Chemistry (R.R. and M.A.R.), and Office of Naval Research (M.A.R.). The crystal structure of Bp-F_3-Nap has been deposited at CCDC with accession number 772735.

Supporting Online Material

www.sciencemag.org/cgi/content/full/328/5985/1547/DC1
Materials and Methods
Figs. S1 to S9
Tables S1 and S2
References

9 March 2010; accepted 29 April 2010
10.1126/science.1189354

Subpolar Link to the Emergence of the Modern Equatorial Pacific Cold Tongue

Alfredo Martínez-Garcia,[1,2,3]* Antoni Rosell-Melé,[3,4] Erin L. McClymont,[5] Rainer Gersonde,[6] Gerald H. Haug[1,2]

The cold upwelling "tongue" of the eastern equatorial Pacific is a central energetic feature of the ocean, dominating both the mean state and temporal variability of climate in the tropics and beyond. Recent evidence for the development of the modern cold tongue during the Pliocene-Pleistocene transition has been explained as the result of extratropical cooling that drove a shoaling of the thermocline. We have found that the sub-Antarctic and sub-Arctic regions underwent substantial cooling nearly synchronous to the cold tongue development, thereby providing support for this hypothesis. In addition, we show that sub-Antarctic climate changed in its response to Earth's orbital variations, from a subtropical to a subpolar pattern, as expected if cooling shrank the warm-water sphere of the ocean and thus contracted the subtropical gyres.

The equatorial Pacific cold tongue is a vivid expression of the ocean's thermocline, the contact between the pools of warm surface water circulating within the subtropical gyres and the colder ocean below. The trade winds drive an east-to-west downward tilt in the thermocline, which causes the thermocline to contact the ocean surface in the eastern Pacific, producing the cold tongue. An "El Niño" occurs when weaker trades allow the thermocline tilt to relax toward the horizontal, causing the cold tongue to disappear (*1*, *2*). The cold tongue is also sensitive to the mean depth of the thermocline (*3*), which can change on longer time scales, deepening in response to reduction in the meridional temperature gradient (*4*–*6*). If the thermocline deepens from its present position, the eastern cold tongue might eventually disappear.

Several authors have suggested that the warm-water volume was greater and the cold tongue absent in warm Pliocene times (*5*–*9*), with the cold tongue emerging only after adequate cooling had occurred. The existing paleotemperature data sets from the equatorial Pacific indicate that the emergence of the cold tongue during the Pliocene-Pleistocene transition was probably a multistage process that involved a different temporal behavior and signature at different locations and latitudes. The sea surface temperature (SST) reconstructions from the eastern part of the present-day cold tongue [Ocean Drilling Program (ODP) Site 846] seem to indicate that the latitudinal temperature gradient along the equator started to emerge around 4.3 million years ago (Ma) (*10*). However, the multiproxy paleotemperature estimates (based on alkenones and Mg/Ca paleothermometers) from a record located several hundred kilometers toward the west (ODP Site 847) show very little change at that time (*7*, *11*), indicating that the cold tongue, if present, was probably smaller than today. Indeed, the paleotemperature data from ODP Site 847 suggest that the cold tongue expanded toward its present configuration in the interval from ~1.8 to ~1.2 Ma (*7*), during what would appear to be a time of relatively stable polar climate and glacial ice volume (*12*). If the development of the modern cold tongue was driven by thermocline shoaling, it should have been accompanied by an equatorward contraction of the thermocline's polar margins, which is a second expression of the volume of warm ocean water (*5*, *6*). However, the paleoceanographic

[1]Geological Institute, ETH Zürich, 8092 Zürich, Switzerland. [2]DFG-Leibniz Center for Surface Process and Climate Studies, Institute for Geosciences, Potsdam University, D-14476 Potsdam, Germany. [3]Institut de Ciència i Tecnologia Ambientals, Universitat Autònoma de Barcelona, Bellaterra, 08193 Catalonia, Spain. [4]Institució Catalana de Recerca i Estudis Avançats, Barcelona, 08010 Catalonia, Spain. [5]School of Geography Politics and Sociology, Newcastle University, Newcastle upon Tyne NE1 7RU, UK. [6]Alfred Wegener Institute for Polar and Marine Research, D-27568 Bremerhaven, Germany.

*To whom correspondence should be addressed. E-mail: alfredo.martinez-garcia@erdw.ethz.ch